Tangential Flow of FENE-P Viscoelastic Fluid within Concentric Rotating Cylinders

L. Shirazi[1];M.Mirzazadeh[2] ; F. Rashidi[3]

ABSTRACT

An analytical solution is presented for the steady state and purely tangential flow of a nonlinear viscoelastic fluid obeying the constitutive FENE-P model in a concentric annulus with inner cylinder rotation. The effect of fluid elasticity (Weissenberg number), the extensibility parameter of the model (L^2) and aspect ratio on the velocity profile and production of friction factor and Reynolds number ($f'\mathrm{Re}$) are investigated. The results show the strong effect of viscoelastic parameters on the velocity profile. The results also show that $f'\mathrm{Re}$ decreases with increasing fluid elasticity and radius ratio.

KEYWORDS

FENE-P constitutive equation, annular flow, tangential flow, analytical solution, viscoelastic fluid.

1. INTRODUCTION

Tangential flows of non-Newtonian fluids within annuli have wide range of engineering applications such as to journal bearings, commercial viscometers, swirl nozzles, chemical and mechanical mixing equipment and electrical motors [1].

An extensive bibliography of work on the flow of non-Newtonian liquids through annular channels is given in the recent paper by Escudier et al [2]. The flow of a Casson fluid between two rotating cylinders was studied by Batra and Das [3] and a summary of laminar flow of non-Newtonian fluids in a rotating annulus was reported by Batra and Eissa [4]. Flow of a fluid obeying the Robertson-Stiff model was investigated by Eissa and Ahmad [5] while Rao [6] reported results for the flow of a Johnson-Segalman fluid between rotating co-axial cylinders. Khellaf and Lauriat [7] analyzed the convective heat transfer characteristics for the flow of a Carreau fluid between rotating concentric vertical cylinders.

The FENE-P model is a non-linear dumbbell model for polymeric liquids, which was derived for dilute solutions but may be extended to semi-dilute and concentrate solutions following the ideas of the encapsulated dumbbell model [8]. This model is based on the kinetic theory for finitely extensible dumbbells.

The model exhibits shear-thinning while its elongational viscosity remains finite for all rates of extension. With a single relaxation time, the model performs remarkably well over a wide range of shear rates; its asymptotic behavior for large shear rates makes it unnecessary to add a significant Newtonian viscosity to maintain a stable fluid behavior.

The fully developed dynamical isothermal solution for the FENE-P model has been derived by Oliveria [9] but the literature is very scarce regarding its performance in heat transfer problems.

The objective of the present investigation is to obtain velocity profiles as well as the coefficient of friction using an analytical method to solve the FENE-P model in purely tangential flow between concentric rotating cylinders where the inner cylinder is rotating while the outer cylinder is at rest, for a wide range of Weissenberg numbers and aspect ratios. Analytical solutions for simple flows of viscoelastic fluids are useful, as they allow a complete description of the flow with given explicit expressions, and are also useful to be applied as boundary conditions in computational simulations, with the benefit of allowing a reduction of the size of the computational domain.

[1]L. Shirazi, Ph.D. Student, Department of Chemical Engineering, Amirkabir University of Technology, Tehran, Iran (e-mail: shirazi@cic.aut.ac.ir,l_shirazi@yahoo.com)

[2]M.Mirzazadeh, Ph.D. Student, Department of Chemical Engineering, Amirkabir University of Technology, Tehran, Iran

[3] F. Rashidi, Professor, Department of Chemical Engineering, Amirkabir University of Technology, Tehran, Iran (e-mail: rashidi@aut.ac.ir)

$$V_\theta = V_\theta(r), V_Z = V_r = 0 \quad (1)$$

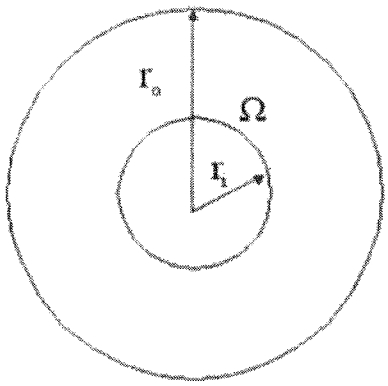

Figure 1: A Schematic diagram of annular geometry

The momentum equation for the $\theta - direction$ is:

$$\rho\left(\frac{\partial V_\theta}{\partial t} + V_r\frac{\partial V_\theta}{\partial r} + V_\theta\frac{\partial V_\theta}{r\partial\theta} + V_z\frac{\partial V_\theta}{\partial z}\right) = -\left(\frac{1}{r^2}\frac{\partial}{\partial r}(r^2\tau_{r\theta}) + \frac{1}{r}\frac{\partial\tau_{\theta\theta}}{\partial\theta} + \frac{\partial\tau_{\theta z}}{\partial z}\right) + \rho g_\theta - \frac{1}{r}\frac{\partial p}{\partial\theta} \quad (2)$$

For the problem under consideration the momentum equation (2) reduces to below:

$$\frac{1}{r^2}\frac{d}{dr}(r^2\tau_{r\theta}) = 0 \quad (3)$$

The dimensionless form of (3) is:

$$\frac{1}{r^{*2}}\frac{d}{dr^*}(r^{*2}\tau^*_{r\theta}) = 0 \quad (4)$$

Following Oliveria [9], the simplified form of the FENE-P model in terms of the extra stress is as follows:

$$\lambda\overset{\nabla}{\tau} + f\tau = 2a\eta_p D \quad (5)$$

where $D = \frac{1}{2}(\nabla V + \nabla V^T)$ or $D = \frac{1}{2}\dot{\gamma}$

Then we arrive at:

$$\lambda\overset{\nabla}{\tau} + f\tau = a\eta_p\dot{\gamma} \quad (6)$$

The function f should now be expressed in terms of the main dependent variable τ [9]:

$$f = 1 + \frac{3a + \frac{\lambda}{\eta_p}tr\tau}{L^2} \quad (7)$$

In these equations the constant model parameters are the polymer viscosity η_p, the relaxation time λ, and the extensibility parameter L^2. The additional parameter a is not an independent parameter; it is a short notation for $a \equiv 1/(1-3/L^2)$ which arises in the derivation. It is related to physical properties by $a = 1 + 3kT/HQ_0^2$ and to the original b parameter [10] by $a = (b+3)/b$.

Sometimes a more simplified version of FENE-P is utilized, in which a = 1 on the assumption that L^2 is large.

The symbol ∇ in (5) is used to denote Oldroyd's upper convected derivative,

$$\overset{\nabla}{\tau} = \frac{D\tau}{Dt} - \tau.\nabla V - \nabla V^T.\tau \quad (8)$$

Where V is the velocity vector, the material derivative is $\frac{D}{Dt} = \frac{\partial}{\partial t} + V.\nabla$, and ∇V^T is the transpose of the velocity gradient.

3. Exact Solution for the FENE-P Model

For steady tangential annular flow (6) reduces to:

$$f\tau_{rr} = 0 \quad (9)$$

$$f\tau_{\theta\theta} = 2\lambda\tau_{r\theta}\dot{\gamma} \quad (10)$$

$$f\tau_{r\theta} = a\eta_p\dot{\gamma} \quad (11)$$

Equation (9) indicates τ_{rr}=0, hence the trace of the stress tensor will be equal to $\tau_{\theta\theta}$. Using (7) for the function f yields:

$$f = 1 + \frac{3a + \frac{\lambda}{\eta_p}\tau_{\theta\theta}}{L^2} \quad (12)$$

By using (10) and (11), the following equation for $\tau_{\theta\theta}$ is obtained:

$$\tau_{\theta\theta} = \frac{2\lambda}{a\eta_p}\tau_{r\theta}^2 \quad (13)$$

The shear rate $\dot{\gamma}$ is obtained by substituting $\tau_{\theta\theta}$ from (13) into (11) and using (12) for the function f:

$$\dot{\gamma} = \frac{\tau_{r\theta}}{a\eta_p}[1+\frac{3a}{L^2}+\frac{2\lambda^2}{a\eta_p{}^2 L^2}\tau_{r\theta}{}^2] \quad (14)$$

where the shear rate $\dot{\gamma}$ is defined by:

$$\dot{\gamma} = r\frac{d}{dr}(\frac{V_\theta}{r}) \quad (15)$$

The dimensionless shear stress is obtained by integrating (4):

$$\overset{*}{\tau}_{r\theta} = \frac{C_1}{\overset{*}{r}{}^2} \quad (16)$$

In (16), the constant C_1 can be obtained using the dimensionless wall shear stress, $\overset{*}{\tau}_{wi}$ on the inner cylinder:

$$\frac{\overset{*}{\tau}_{r\theta}}{\overset{*}{\tau}_{wi}} = \frac{\kappa^2}{\overset{*}{r}{}^2} \quad (17)$$

Combination of (14) and (15) leads to:

$$\overset{*}{r}\frac{d}{d\overset{*}{r}}(\frac{\overset{*}{V}_\theta}{\overset{*}{r}}) = \frac{[(1+\frac{3a}{L^2})+\frac{2}{aL^2}We^2\,\overset{*}{\tau}_{r\theta}{}^2\,]\overset{*}{\tau}_{r\theta}}{a(1-\kappa)} \quad (18)$$

The following normalizations have been used in (18):

$$\overset{*}{r} = \frac{r}{R_o} \quad (19)$$

$$\overset{*}{V}_\theta = \frac{V_\theta}{R_i\Omega_i} \quad (20)$$

$$\overset{*}{\tau}_{r\theta} = \frac{\tau_{r\theta}}{\eta_p R_i\Omega_i/\delta} \quad (21)$$

$$We = \frac{\lambda R_i\Omega_i}{\delta} \quad (22)$$

By substitution of $\overset{*}{\tau}_{r\theta}$ from (17) into (18) and then integration of this equation, the dimensionless velocity profile is obtained, as follows:

$$\frac{\overset{*}{V}_\theta}{\overset{*}{r}} = -\frac{k^2\,\overset{*}{\tau}_{wi}}{a(1-\kappa)\overset{*}{r}{}^2}[\frac{1}{2}+\frac{3a}{2L^2}+\frac{W_e{}^2\kappa^4\,\overset{*}{\tau}_{wi}{}^2}{3aL^2\,\overset{*}{r}{}^4}]+C_2 \quad (23)$$

The dimensionless forms of boundary conditions are as follows:

at $\overset{*}{r}=\kappa$ $\quad \overset{*}{V}_o=1$ (24)

at $\overset{*}{r}=1$ $\quad \overset{*}{V}_o=0$ (25)

By introducing boundary conditions from (24) and (25) into (23) and after mathematical simplification, the following cubic equation is obtained:

$$\overset{*}{\tau}_{wi}{}^3 + p\,\overset{*}{\tau}_{wi} + q = 0 \quad (26)$$

where the constant p and q in (26) are:

$$p=\frac{(\frac{3aL^2}{2}+\frac{9a^2}{2})(1-\kappa^2)}{W_e^2(1-\kappa^6)} \qquad q=\frac{3a^2L^2(1-\kappa)}{W_e^2(1-\kappa^6)\kappa} \quad (27)$$

The real solution of (26) can be expressed as:

$$\overset{*}{\tau}_{wi} = \frac{1}{6}\sqrt[3]{-108q+12\sqrt{12p^3+81q^2}} - \frac{2p}{\sqrt[3]{-108q+12\sqrt{12p^3+81q^2}}} \quad (28)$$

By introducing boundary conditions from (24) or (25) into (23) and using $\overset{*}{\tau}_{wi}$ from (28), the second constant C_2 can be easily obtained.

For the limiting case of a Newtonian fluid ($L^2\to\infty$ or $a\to 1$), (23) reduces to:

$$\frac{\overset{*}{V}_\theta}{\overset{*}{r}} = -\frac{\kappa^2\,\overset{*}{\tau}_{wi}}{2(1-\kappa)}\frac{1}{\overset{*}{r}{}^2}+C_2 \quad (29)$$

By introducing boundary conditions from (24) and (25) into (29), the following relations can be written to obtain $\overset{*}{\tau}_{wi}$ and C_2:

$$\overset{*}{\tau}_{wi} = \frac{-2}{\kappa(1+\kappa)} \qquad C_2=\frac{-\kappa}{(1-\kappa^2)} \quad (30)$$

which is in total agreement with the previous work [8].

An important parameter in engineering calculations is the product of the friction factor and the Reynolds number (Re). The torque friction factor f' can be defined as follows [11]:

$$f' = \frac{\tau_w}{\rho(R_i\Omega_i)^2/\delta} \quad (31)$$

And the rotational Reynolds number as [7] and [12]:

$$\mathrm{Re} = \frac{\rho R_i \Omega_i \delta}{\eta_p} \tag{32}$$

Using these definitions we can derive the following equation for $f'\mathrm{Re}_i$:

$$f'\mathrm{Re}_i = -2\tau_{wi}^{*} \tag{33}$$

where in the above equation subscribe i refers to inner cylinder

4. Results and Discussion

The physical interpretation of the results is facilitated by a few graphs showing the variation of velocity and stresses. Velocity profiles are presented in Fig. 2 for fixed radius ratio $\kappa = 0.5$ and extensibility parameter $L^2 = 10$ and different values of the Weissenberg number (*We*). As can be seen, the velocity gradient near the inner cylinder increases as the Weissenberg number (*We*) increase, i.e., as the shear-thinning behavior of the fluid increases. In other words, by increasing fluid elasticity, the viscosity function of fluid decreases (as will be discussed on the next paragraphs) which results in increases in velocity gradient. Also, the maximum velocity gradients are concentrated near inner cylinder due to rotation of inner cylinder.

The shear thinning behavior of FENE-P fluid can be explained by obtaining the viscosity function of FENE-P fluid. Although the viscosity parameter of this model (η_p) is a constant, the viscosity function (which is defined in (34)), is not a constant and tends to decrease with $\dot{\gamma}$:

$$\eta(\dot{\gamma}) = \frac{\tau_{r\theta}}{\dot{\gamma}} \tag{34}$$

By substitution of (14) into (34) we arrive at:

$$\frac{\eta(\dot{\gamma})}{\eta_p} = \frac{a}{[1 + \frac{3a}{L^2} + \frac{2\lambda^2}{a\eta_p^{\,2} L^2}\tau_{r\theta}^{\,2}]} \tag{35}$$

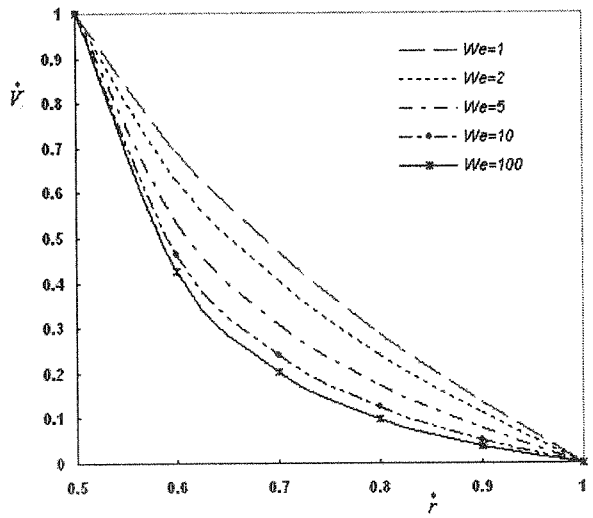

Figure 2: Effect of Weissenberg number (*We*) on the velocity profile for κ=0.5 & $L^2 = 10$

Fig. (3) shows the flow curve of FENE-P fluid where the viscosity function of fluid (which is scaled with model viscosity parameter, η_p) is given as function of dimensionless shear rate (equal to $\dot{\gamma}\lambda$, and so can be viewed as a Weissenberg number). As can be seen from this figure, by increasing the shear rate the viscosity of fluid decreases and for large value of shear rate the viscosity decreases as $\eta(\dot{\gamma}) \sim \dot{\gamma}^{-2/3}$ which is in agreement with the previous works (e.g., [9] and [13]).

The shear-thinning behavior of the fluid also is shown in Fig. 4. This figure indicated that the shear stresses decrease inside the annular gap by increasing Weissenberg number (*We*). This is because by increasing fluid elasticity, the viscosity function of fluid decreases (as shown in Fig. (3)). Therefore the magnitude of shear stress decreases in the annular space. Also, as can be seen from this figure, the magnitude of shear stress decreases inside the annular gap with increasing dimensionless radius, as it arises from Eq. (17).

The effect of extensibility parameter (L^2) on the velocity profile for fixed $We = 2$ and $\kappa = 0.5$ is shown in Fig. 5.

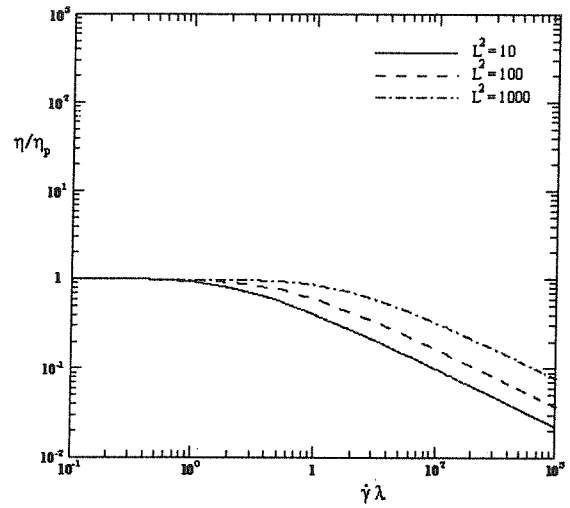

Figure 3: Shear viscosity of FENE-P fluid in steady simple shear flow for $L^2 = 10$

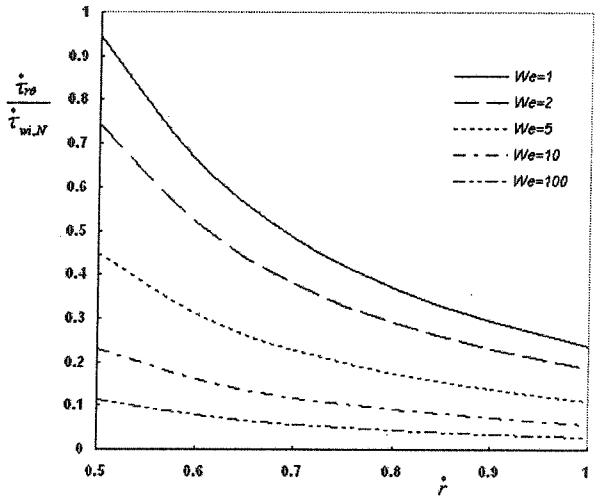

Figure 4: Variation of dimensionless shear stress (which is normalized with dimensionless Newtonian wall shear stress) inside the annular gap as a function of Weissenberg number (We) for κ =0.5 & L^2=10

Also, the influence of the radius ratio on the velocity profile is shown in Fig. 6. The results show that the profiles become increasingly linear with increasing radius ratio, κ. In the narrow gap, as we know, the shear stress is approximately constant then the velocity profile tends to take linear form.

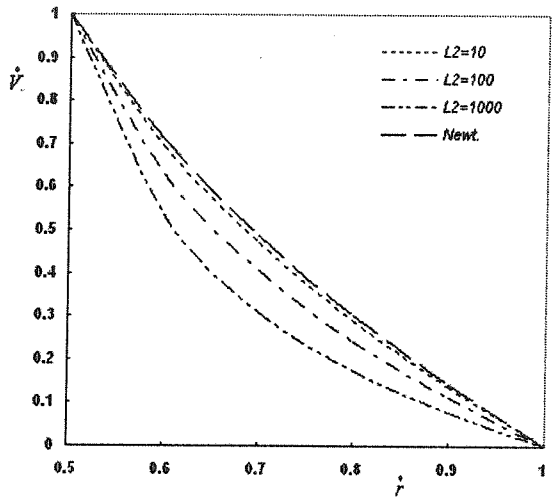

Figure 5: Effect of extensibility parameter (L^2) on the velocity profile for $We = 2$ and κ =0.5

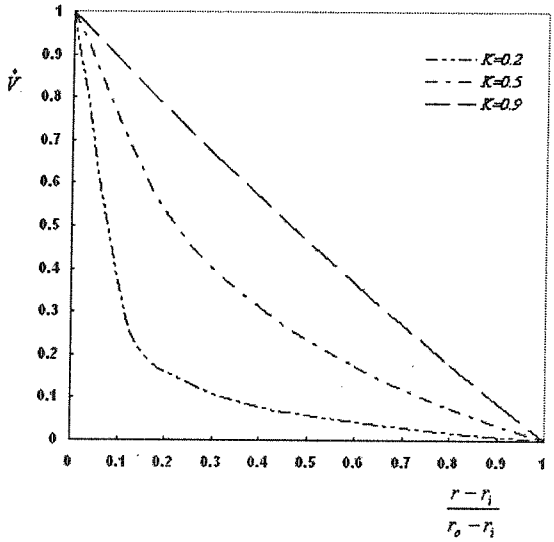

Figure 6: Effect of the radius ratio on velocity profile for $We = 2$ and L^2 =10

The effect of fluid elasticity on the variation of normal stress is also interesting in the analysis of the viscoelastic fluid flow. To perform such analysis, we rewrite (13) in the dimensionless form as below:

$$\overset{*}{\tau}_{\theta\theta} = \frac{2We}{a}\overset{*2}{\tau}_{r\theta} \qquad (36)$$

Fig. (7) shows the effect of Weissenberg number on the radial profile of dimensionless normal stress ($\overset{*}{\tau}_{\theta\theta}$). As can be seen from this figure, the normal stress ($\overset{*}{\tau}_{\theta\theta}$) does not behave monotonically, in other words, $\overset{*}{\tau}_{\theta\theta}$ first increases by increasing Weissenberg number but when Weissenberg number goes to higher values, it shows the

opposite trend (as shown in Fig. (8), where the value of $\tau^*_{\theta\theta}$ on the inner cylinder is shown against the Weissenberg number). This is because $\tau^*_{\theta\theta}$ is affected by both fluid elasticity (directly proportional to *We*, as can be seen from (36)) and by shear thinning behavior of fluid (as shown in Figs. (3) and (4), where $\tau^*_{r\theta}$ decreases by increasing fluid elasticity). For this reason, it would be better to plot the normal stress scaled with wall shear stress as shown in Fig. (9). As can be seen from this figure, the shear thinning effect is removed from the normal stress profile and the normal stress variation is now monotonic with Weissenberg number. A similar result has been obtained previously by Oliveira [9] for pipe and slit flow of FENE-P fluid (Fig. 4a in his work), Mostafaiyan et. al. [14] for annular flow of Giesekus fluid (Fig. 2a in their work) and also by Oliveira et. al. [15] for channel and pipe flow of PTT fluid (Fig. 4b in their work).

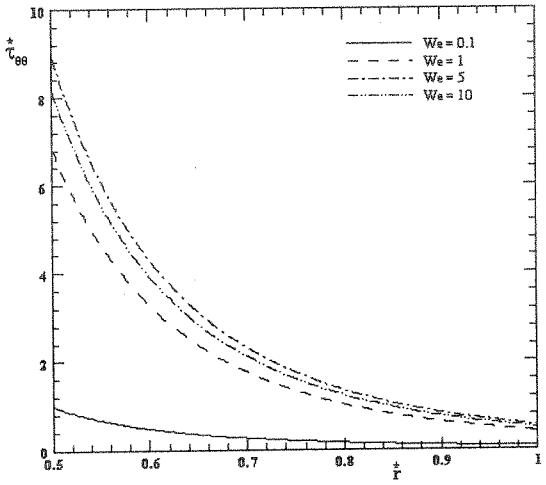

Fig. 7: The effect of Weissenberg number on radial profile of dimensionless normal stress ($\tau^*_{\theta\theta}$) for constant values of κ=0.5 & L^2=10

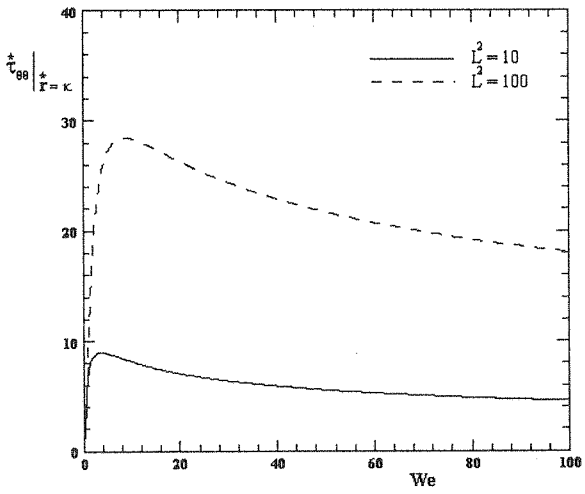

Fig. 8: $\tau^*_{\theta\theta}\Big|_{r^*=\kappa}$ vs. We for constant values of k=0.5

Fig. 10 shows the effect of the Weissenberg number (*We*) on f'Re which is normalized with the corresponding Newtonian value ($f'\mathrm{Re}_{i,N} = 4/\kappa(1+\kappa)$) for the various radius ratio. The decrease in f'Re with increasing the Weissenberg number (We) is again attributable to the shear-thinning behavior of the FENE-P fluid. As shown in the definition of f'Re (see Eq. (23)), the product of friction factor and Reynolds number (f'Re) is proportional to dimensionless wall shear stress (τ^*_{wi}). Therefore the effect of fluid elasticity on f'Re is similar to the effect of fluid elasticity on shear stress (as shown in Fig. (4)). As can be seen from this figure, as Weissenberg number approaches zero the f'Re values are in agreement with those for a Newtonian fluid [7], [11] and [12].

The Taylor number *Ta* is an alternative to the rotational Reynolds number and the definition adopted here is the same as that used by Escudier et al [2] for the case of inner cylinder rotation:

$$Ta = \left(\frac{\rho\Omega}{\eta_P}\right)^2 R_i\delta^3 \qquad (37)$$

Using torque friction factor, f', from (31) and Taylor number, *Ta*, from (37) we arrive the following equation:

$$f'\sqrt{Ta} = -2\tau^*_{wi}\sqrt{\frac{1-\kappa}{\kappa}} \qquad (38)$$

which can be calculated in the same way as f'Re.

For the limiting case of a Newtonian fluid, with τ^*_{wi} from (30) substituted into (35), we arrive at:

$$f'\sqrt{Ta} = 4\sqrt{\frac{1-\kappa}{\kappa^3(1+\kappa)^2}} \qquad (39)$$

which is in agreement with the previous work [11].

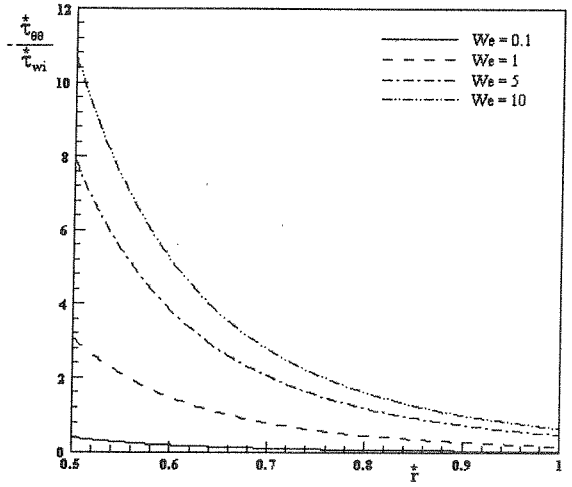

Fig. 9: Dimensionless normal stress profiles for varying Weissenberg number normalized with dimensionless wall shear stress ($\overset{*}{\tau}_{wi}$) for constant values of κ =0.5 & L^2=10

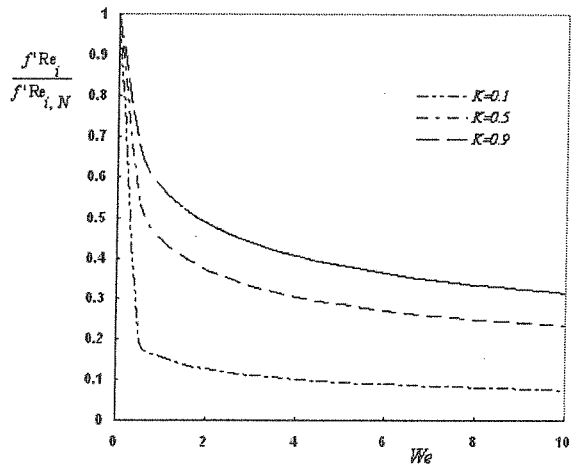

Figure 10: Effect of Weissenberg number and radius ratio (κ) on the ratio of the viscoelastic to the Newtonian friction factor ($f'\mathrm{Re}_i / f'\mathrm{Re}_{i,N}$)

5. Conclusion

An analytical solution has been derived for the steady-state, purely tangential flow in a concentric annulus with inner cylinder rotation of a viscoelastic fluid obeying the complete form of the FENE-P constitutive equation. The results include the profiles of all relevant stresses, the tangential velocity and the viscosity across the gap. Expressions are also given for the viscometric viscosity and shear and normal stress, as a function of the model parameters, in steady shear flow. The results show that:

1. Increasing the Weissenberg number increases the velocity gradient near the inner cylinder and so decreases the viscometric viscosity of the fluid (i.e., the fluid behavior is increasingly shear-thinning)

2. f'Re decreases with increasing fluid elasticity and radius ratio, which indicates that the required torque for rotation of a cylinder in tangential flow of viscoelastic fluid is much lower than its corresponding value for Newtonian fluid.

3. The normal stress profile is found to vary in a non-monotone way with the dimensionless parameter characterizing viscoelasticity, the Weissenberg number.

6. Nomenclature

C_1	Constants in shear stress profile (equation (16))
C_2	Constants in velocity profile (equation (23))
f'	Rotational friction factor, $\tau_w / (\rho V_c^2/2)$
f	Function for FENE-P model
p	Constant [see Eqs. (26), (27) and (28)]
q	Constant [see Eqs. (26), (27) and (28)]
r	Radial coordinate
z	Axial coordinate
R_i	Inner cylinder radius
R_o	Outer cylinder radius
$\overset{*}{r}$	non-dimensional radial coordinate, r / R_o
Re	Rotational Reynolds number, $\rho R_i \Omega_i \delta / \eta_p$
Ta	Taylor number, $(\rho\Omega / \eta_P)^2 R_i \delta^3$
V	Tangential Velocity
$\overset{*}{V}_\theta$	Non-dimensional velocity, $V_\theta / (R_i \Omega_i)$
We	Weissenberg Number, $\lambda R_i \Omega_i / \delta$
a	A constant and independent parameter of the FENE-P model
L^2	Extensibility parameter of the FENE-P model

Greek Letters

δ	Annular gap width, R_o- R_i
$\dot{\gamma}$	Shear stress tensor
η_p	Polymer viscosity coefficient of the FENE-P model
η	Shear viscosity, $\tau_{r\theta} / \dot{\gamma}$
κ	Radius ratio, R_i/R_o
λ	Relaxation time in FENE-P model
Ω	Angular velocity of inner cylinder
ρ	Density
θ	Tangential coordinate
τ	Stress tensor
$\overset{*}{\tau}_{r\theta}$	Non-dimensional shear stress, $\tau_{r\theta} / (\eta_p R_i \Omega_i / \delta)$
$\overset{*}{\tau}_{wi}$	Non-dimensional wall shear stress on the inner cylinder

Superscripts

T	Transpose of tensor
*	Refers to dimensionless quantities

Subscripts

i	Refers to inner cylinder
N	Refers to Newtonian value
o	Refers to outer cylinder
w	Refers to wall value

7. REFERENCES

[1] [1] D.M. Maron, S. Cohen, "Hydrodynamics and heat/mass transfer near rotating surfaces," Adv. Heat Transfer, vol. 21, pp. 141–183, 1991.

[2] [2] M.P. Escudier, P.J. Oliveria, and F.T. Pinho, "Fully developed laminar flow of purely viscous non-Newtonian liquids through annuli including the effects of eccentricity and inner cylinder rotation," International Journal of heat and Fluid Flow, vol. 23, No. 1, pp. 52-73, 2002.

[3] [3] R.L. Batra, B. Das, "Flow of Casson fluid between two rotating cylinder," Fluid Dynamics Research, vol. 9, pp. 133-141, 1992.

[4] [4] R.L. Batra, M. Eissa , "Helical Flow of a Sutterby model Fluid," Polym. – Plast. Technol. Eng., vol. 33, pp. 489-501, 1994.

[5] [5] M. Eissa, S. Ahmad, "Forced convection Heat transfer of Robertson – stiff fluid between two coaxial rotating cylinders," International communication in Heat and Mass Transfer, vol. 26, pp. 695-704, 1999.

[6] [6] I.J. Rao, "Flow of a Johnson-Segalman fluid between rotating coaxial cylinders with and without suction," International Journal of Non-Linear Mechanics, vol. 34, pp. 63-70, 1999.

[7] [7] K. Khellaf, G. Lauriat, "Numerical study of heat transfer in a non-Newtonian Carreau-fluid between rotating concentric vertical cylinders," Journal of non-Newtonian Fluid Mechanics, vol. 89, pp. 45-61, 2000.

[8] [8] R.B. Bird, C.F. Curtiss, R.C. Armstrong , O. Hassager, Dynamics of Polymeric Liquids, Kinetic Theory, vol. 2, second ed., New York: Wiley, 1987.

[9] [9] P.J. Oliveria, "An exact solution for tube and slit flow of a FENE-P fluid," Acta Mech., vol. 158, pp. 157-167, 2002.

[10] [10] R.B. Bird, P.J. Dotson, N.L. Johnson, "Polymer solution rheology based on a finitely extensible bead-spring chain model," J. Non-Newtonian Fluid Mech., vol. 7, pp. 213-235, 1980.

[11] [11] J.H. Vohr, "An experimental study of Taylor vortices and turbulence in flow between eccentric rotating cylinder," Journal of Lubrication Technology, vol. 90, pp. 285-296, 1986.

[12] [12] Jr.C. Gazley, C.S. Monica, "Heat transfer characteristics of the rotational and axial flow between concentric cylinders," Transactions of The ASME, paper number 56-A-128, pp. 79-90, November 1956.

[13] [13] B. Purnode, M. J. Crochet, "Polymer solution characterization with the FENE-P model," Journal of Non-Newtonian Fluid Mech. Vol 77, pp. 1 – 20, 1998.

[14] [14] M. Mostafaiyan, Kh. Khodabandehlou, F. Sharif, "Analysis of a viscoelastic fluid in an annulus using Giesekus model," Journal of Non-Newtonian Fluid Mechanic vol 118, pp. 49-55, 2004.

[15] [15] P.J. Oliveira, F.T. Pinho, "Analytical solution for fully developed channel and pipe flow of Phan- Thien- Tanner fluids," Journal of Fluid Mechanics, vol 387 pp. 271-280, 1999.